Measurement of Initial Conditions of a Kerosene Spray from a Generic Aeroengine Injector at Elevated Pressure

S. Freitag*, U. Meier, J. Heinze, T. Behrendt and C. Hassa
German Aerospace Center - DLR, Institute of Propulsion Technology
Linder Höhe, 51147 Cologne, Germany

Abstract

Ab initio prediction of aeroengine sprays at realistic conditions is currently not feasible and will remain so for a significant time to come. As a partial solution to the problem, experimental data are generated to validate advanced combustion codes. For that purpose a generic injector was built and operated in an optical single sector combustor. Phase Doppler Anemometry and Mie Scattering were used. The in house algorithm that performs the on line measurement of the measuring volume was modified to suit the experimental setup. Measurements were performed at 4bar and 10bar. Good mass flux density profiles can be obtained within the lift-off distance of the flame.

Introduction

European aviation has pledged to reach the ACARE goals of environmental compatibility in the year 2020. The goal of reduction of NOx by 80% must be reached by improved combustor technology. In view of the time required to achieve the necessary technological readiness, the transfer of a significant part of the development process into computer simulation is very desirable. As of today, the biggest impediment to that is the unavailability of reliable methods for spray prediction. Although with Level Set or Volume of Fluid, methods exist that can predict atomization, computers are just not quick enough today to calculate through the atomization process at the small scales that are created by modern air blast atomizers for aeroengines. Hence intermediate solutions have to be pursued and this contribution is part of such an approach. The spray initial conditions are measured for a generic atomizer that exhibits a spray similar to an aeroengine spray but without the features assuring airworthiness. With these measurements incorporated in the combustion codes as initial conditions, their ability to reproduce the spray combustion in a generic combustor at relevant conditions is tested.

For the formulation of initial conditions of the spray in a time averaged form, PDA measurements of volume flux densities of the liquid, drop sizes, drop velocities and their RMS values in the coordinate directions are desirable. Of those, the flux density measurement is the most important, as it is directly coupled to the fuel placement, yet it is the most difficult to achieve, as in principle all particles need to be counted and the instantaneous measurement volume needs to be measured. This is only possible if all particles are spherical and the number density low enough to allow a complete count. For combusting sprays, this leads to a position, where combustion has already done part of its work and the conditions measured are no longer initial. In this contribution that problem was circumvented in part by creating a lifted flame as in the practical case of lean burners, which leaves the spray for some time to the evaporation driven by the temperature difference to the preheated air only. Hence a compromise on the position of the measurement needs to be made, as well as numerous others on the PDA setup. Here together with the results, we want to share our method as well as the choices we made, which are in no way the singular possible solution to the problem.

Test section and test conditions

Figure 1a shows a schematic view of the generic burner, which was designed and manufactured by DLR and some of its details. The two air flows are co-rotating. Kerosene is supplied by two opposite fuel lines to an annular fuel gallery and from there to a vertical slot through a circular array of 36 orifices with 0.2 mm^2 area each. The pressure drop across these metering holes, along with the length of the vertical slot, should result in a good circumferential homogeneity of the fuel as it exits the end of the slot, which is inclined at an angle of 31°. The diameter of the inner air channel is 15 mm; the exit diameter of the outer channel is 24 mm.

The burner was operated in the Single Sector Combustor (SSC). The combustion chamber is schematically shown in figure 1b. It features a square cross section of 102 x 102 *mm* and a length of 264 *mm*. Electrically preheated compressed primary air – shown in yellow – is supplied to the plenum upstream of the combustion chamber through a sonic nozzle, which is used for metering the air mass flow. Additional preheated air is diverted from the primary air supply and guided to the windows for cooling. The secondary air supply shown in the figure 1b was not used in these experiments. Burner and window film cooling air are both controlled by sonic nozzles;

* Corresponding author: stefan.freitag@dlr.de

therefore, the ratio of the air flows was always constant, regardless of the absolute burner air mass flow, which is a function of the variable operating parameters combustor pressure, injector pressure loss and air preheat temperature. The ratio of the burner and film cooling air for the used test case A and B are shown in table 1. The first case A at low pressure and low preheat temperature is corresponding to idle conditions of an engine, whereas for case B the higher pressure and preheat temperature is nearer to a cruise condition.

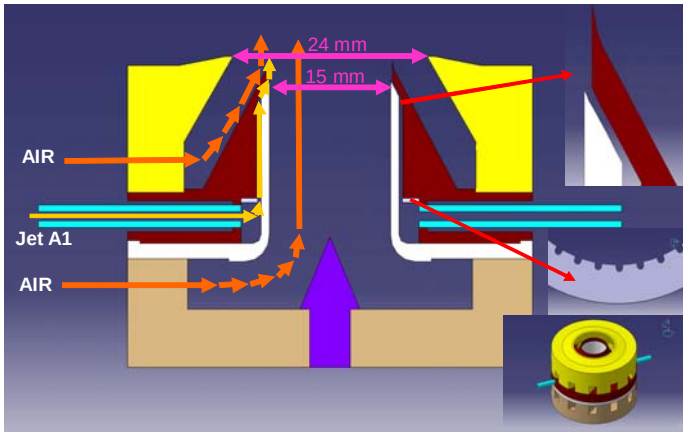

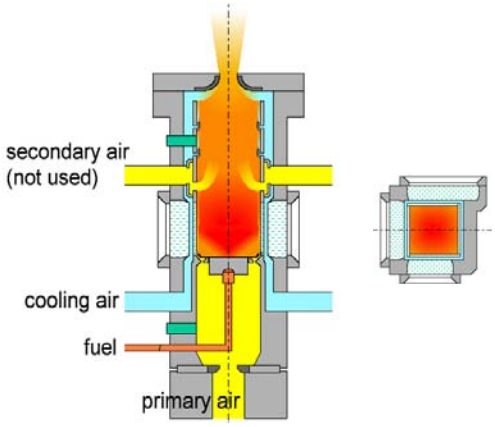

Figure 1a. Schematics of the burner; on the right: details of the fuel exit slot (top), the metering holes (center), and a 3D view of the assembly(bottom)

1b. Schematics of the Single Sector Combustor; right: cut through optical section

The combustor pressure is controlled by another sonic nozzle forming the choked exit of the combustor, along with additional cooling air (blue) which enters the flame tube just upstream from the exit, after cooling the outside of the windows in the optical section and the liner downstream of the windows.

The entire rig is mounted on a three-axis traversing stage which allows positioning with respect to the laboratory reference frame with an accuracy of 0.1 mm. The PDA transmitting and receiving optics were mounted on a fixed frame, and variation of the measurement location was achieved by traversing the rig relative to the optical setup.

Table 1. List of test conditions cases

Case	Air pressure p [MPa]	Air Preheat temperature T [K]	Burner pressure loss [%]	Mass flux preheated air $\dot{m}$ [g/s]		Liquid Fuel [g/s]
				Burner	Film cooling	
A	0.4	550	3	60	17	3.0
B	1.0	650	3	140	39	6.8

To insert the Fuel into the burner, the fuel pipe has to be installed in the plenum which is exposed to the preheated air. Consequently the fuel is preheated even before entering the burner. To get information about the temperature of the fuel, a thermocouple was installed in the wall of the slot following the orifices.

Measurement setup

For the selection of a PDA measurement setup for combustion chambers, consideration of some specific aspects is mandatory. One of these is the effect of the dense-spray. Caused by the secondary scattering at the drops, the beam overlapping is more inexact. Thus the detection of the diffused signal gets worse which in turn leads to a lower signal to noise ratio (SNR). With a higher laser light intensity, a higher SNR can be obtained and hence a lower effect of the dense spray.

To get high laser intensity in a defined local area of the measuring volume a beam expander with an expansion factor of 1.98 and a front lens with a small focal length of 310 mm was chosen. Taking into account the transmission losses by the chamber window, the laser power in the measuring volume of diameter D_M = 76 µm was around 80 mW per beam at wave length λ = 514 nm as shown in table 2. The small measuring volume yields another advantage as it minimizes the probability that more than one droplet is in the detection area at the same time which promotes higher validation rates.

Another consideration is the beam-steering effect caused by density fluctuations especially at higher temperature and higher pressure in combustion chambers [2], [3] and effects of lower SNR and additional fluctuation of the measuring particle diameter [4]. The incomplete overlapping of the laser beams might be reduced by using a long focal length for the transmitter front lens or dispensing the beam expander to get a larger measuring volume with a larger diameter D_M and hence higher probability of beam overlap. However this would decrease the local laser light intensity. The beam-steering effect increases with longer path length of laser beams and receiving cone in the zone of temperature fluctuations at high air density [3], [4], which is limited by the chamber. With no changes to the optical setup and increased laser power, the effect of beam steering decreases with higher SNR [4].

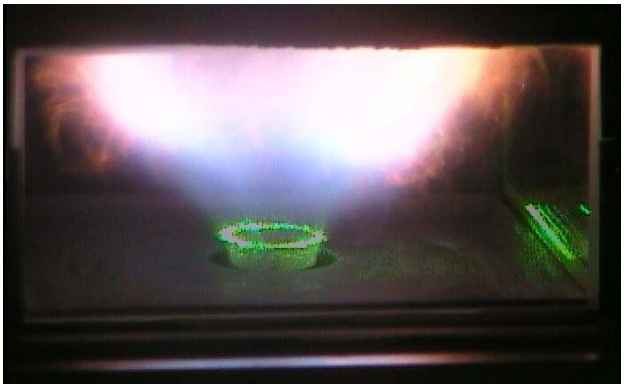

Figure 2a. Photograph of the lifted flame of the burner with a horizontal laser light sheet through the annular dense spray

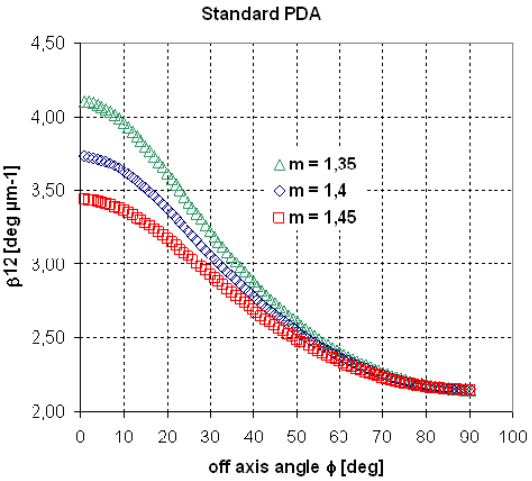

2b. Calculated dependency of phase shift factor and off axis angle for different relative refractive indices of fuel to air for the chosen setup

In figure 2a a photograph of a lifted flame of the above mentioned burner is shown. The lifted flame is stable and has low amplitude of fluctuation. There is a hot region in the area of flame and a dense spray region near the fuel exit slot of the burner. Hence the burner is well adapted for a PDA measurement in the region of the dense spray. With the assumption of a very fine atomization with a high droplet number density spray, a measurement setup strategy with high laser intensity was chosen.

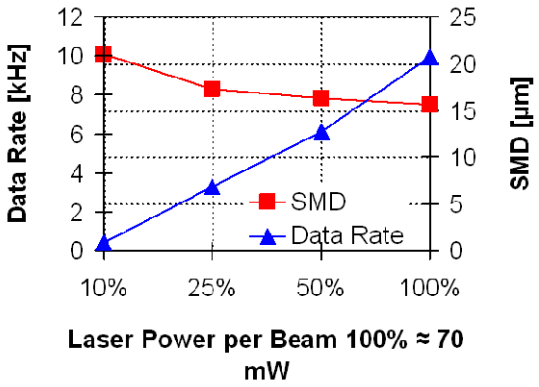

Figure 3a. Relation of SMD and data rate versus the laser power at position $P_{x,y,z}$ (12; 8; 9)

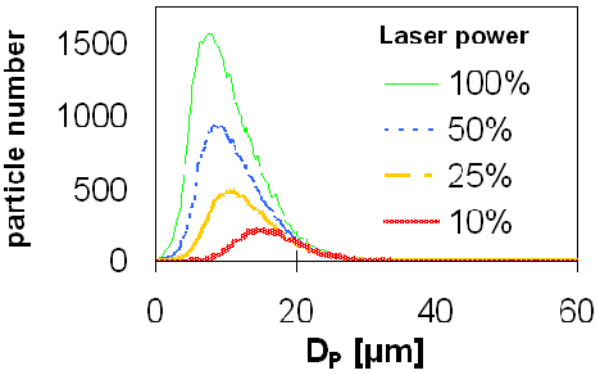

3b. Drop size number distribution at the position $P_{x,y,z}$ (12; 8; 9) with a variation of laser power at a constant elapsed time *te*

Another effect to be taken into account while characterizing evaporating sprays in general is the temperature dependency of the liquid's refractive index. In figure 2b the dependency of phase shift factor and off axis angle for different relative refractive indices of fuel and air for the chosen optics and settings is shown. The different

refractive indices from 1.35 to 1.45 refer to different fuel temperatures from 300 K to 510 K calculated with a function from [5]. With increasing off axis angles the influence of a changing refractive index on the phase shift factor β is diminished. Hence for correct diameter measurements in evaporating sprays an off axis angle close to the Brewster's angle is strongly recommended. From this also results a smaller measuring volume due to the reduced projected slit length, see figure 5. A small measuring volume is a requirement for measurements in dense sprays as it lowers the probability of two or more droplets being in the measuring volume at the same time. This is a desired effect. On the other hand a large off-axis angle has two disadvantages. The choice of the receiving optics is limited to a conventional PDA receiver. Operating a Dual PDA with large off axis angles will lead to 2π-ambiguities caused by strong fluctuations of the phase difference of the planar PDA for small droplets as shown in [1]. Additionally the intensity of the scattered light is decreasing by up to an order of magnitude, depending on the optical setup, while changing the off axis angle from 30° to 68°, see [6]. So measurements with a large off axis angle require high laser intensity in the measuring volume to avoid droplet size distributions biased towards larger droplets.

A preliminary test was conducted to check, if the used laser could provide sufficient light intensity in the measuring volume. A position in the dense spray at x = 12 mm, y = 8 mm and z = 9 mm was chosen to analyse the effect of laser power on the measured droplet diameter distribution. At this position there is a long path length of the laser beams through the combustor, hence it was assumed that there were strong beam steering effects. The influence of varying laser intensity on the measured SMD and the data rate is shown in figure 3a. At power settings of 50% and above the curve of the SMD shows an asymptotic behaviour. The influence of the laser intensity on the detection of small droplets is shown in figure 3b. At power settings below 50% the detection threshold is shifted significantly towards larger droplets ending at a threshold of $D_p \approx 10\mu m$ for 10% laser intensity. So the laser system used is qualified for PDA measurements with a large off axis angle.

The beam arrangement around the combustion chamber is shown in figure 4a and 4b. With a 2D optic a measurement on two traverse directions is needed to get all three velocity components as shown in figure 4a. With the used large off axis angle at $\phi = 68°$ only half traverses are possible, the beams being cut of by the pressure casing for the other half. To minimize the beam-steering effect it is useful to traverse the measuring volume with a path length of the beams in the combustion chamber which is as low as possible. The arrangement in figure 4a was optimized in this regard. A 3D CAD tool was used to identify the traverse path positions avoiding shadow effects of the optics caused by the casing. For a measurement of the traverse path near the burner exit it was necessary to tilt the measurement plane to avoid a shadow effect of the receiving cone as shown in figure 4b.

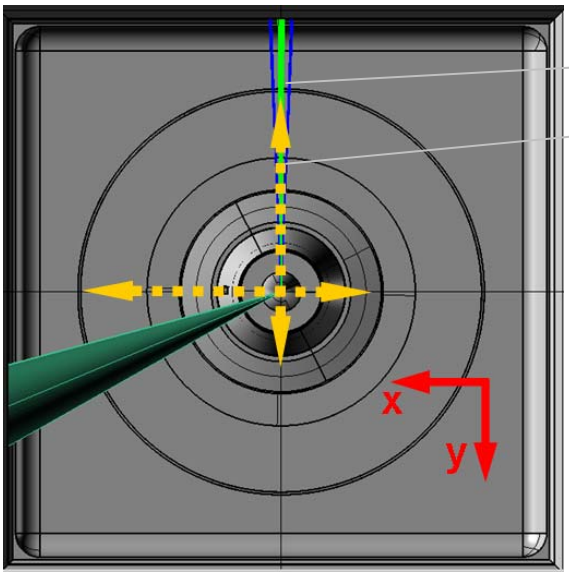

Figure 4a. Top view on beam arrangement at the combustion chamber with marking of traverse path

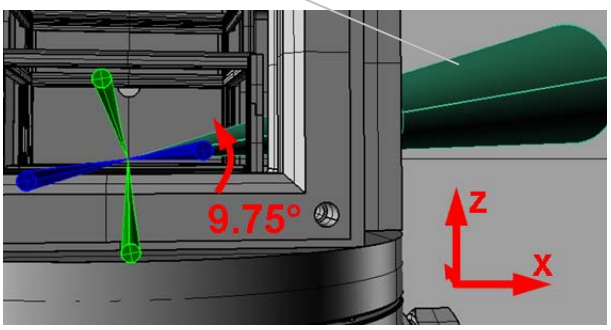

4b. Tilting angle at 9.75° of the measurement plane around the optical axis of the transmitter

The point of origin is fixed at the burner plate in z-direction and at the axis of the burner the x-y direction is defined in figure 4. Here, a Cartesian coordinate system is chosen to draw conclusions from the data quality related to the measured points and the optical alignment. The droplet diameter D_P and the velocity components u and v were measured on 7 half-traverses from 7 mm to 30 mm in z-direction alongside the x-direction. To get the tangential velocity component w, 6 half-traverses from 7 mm to 25 mm in z-direction alongside the y-direction

were measured additionally. The measured extension of these traverses was limited by the particle concentration and the restrictions of the chamber. The abort criterion of a measurement was set to 120 seconds and 50000 validated samples, whichever comes first.

The planar Mie scattering signal, which represents the distribution of the liquid fuel, was generated using pulsed laser light at 532 nm from a frequency-doubled Nd:YAG-laser (Spectra Physics) with a pulse duration of approximately 10 ns. The laser beam was formed to a light sheet with 48 mm height and 0.2 mm waist thickness. Mie scattering was recorded at right angle by a CCD camera (FLAMESTAR II, LaVision). The non-uniformity of the light intensity distribution across the laser sheet was accounted for by normalizing each Mie image with the corresponding light sheet intensity distribution. The latter was monitored by exciting laser-induced fluorescence in a quartz cell filled with laser dye solution by a fraction of the light sheet which was split off the main beam before entering the combustor. The fluorescence intensity distribution was recorded by a second camera and used for normalization of the Mie signal.

Table 2. Specification of PDA system

Transmitting optics			**Receiving optics**	
Wavelength of laser beams	514.5 nm	488 nm	Off axis angle	68°
Diameter of laser beams	1.35 mm		Focal length of front lens	310 mm
Beam expander ratio	1.98		Width of the receiving slit	100 µm
Focal length of front lens	310 mm		Max. particle diameter	119 µm
Measuring volume diameter	76 µm	72 µm	Covariance processor Dantec 57X80	
Fringe spacing	6.2 µm	5.9 µm	Max. velocity bandwidth (45MHz)	274 m/s
Laser light intensity per beam in the measuring volume	80 mW	70 mW	Optical frequency shift	40 MHz

Volume Flux Calculation

The following equation describes the fuel volume flux at the elapsed time *te* with the summation of particle diameters D_P and reference area A_{ref} in a specific coordinate *j* for each validated particle *i*:

$$Flux_j = \frac{\pi}{6 \cdot te} \sum_i \frac{D_{P,i}^3}{A_{ref,j,i}} . \quad (1)$$

$A_{ref,x}$ is a function of the projected slit width, the measuring volume diameter D_M and the particle trajectory. The light intensity in the measuring volume has a Gaussian distribution. From it this follows that the intensity of the detected signal depends on size and position of the particle in the measuring volume and hence the size of measuring volume depends on D_P. Thus the relation of D_M and D_P has to be calculated from the measured data.

The software of the PDA contains flux and concentration algorithms [6], which are based on the approach presented in [7]. A 2D-trajectory consideration is included in these algorithms, but the probe volume diameter calculation is working on the assumption, that the main velocity direction is normal to the off axis plane. A probe volume diameter calculation, which based of a velocity direction in line with the off axis plane and normal to the optical axis of the transmitter, is included in [8]. A combination of 3D-trajectories and any off axis angles is demonstrated in [1]. Following [8] and [1], a 2D algorithm was created for this study.

An approach to get the measuring volume diameter $D_M(D_P)$ is a correlation of the measured burst lengths bl_{meas} with the measured velocity trajectories and the existing geometry of the probe volume to find a rectified burst length bl_{true}. Here the measured burst length is defined as $bl_{meas} = t_{res} (u^2 + v^2)^{1/2}$. For the following considerations bl_{meas} is a mean value and refers to a particle size class.

For the reason of a slit in the receiving optics and its dependences on the off axis angle ϕ, the detection volume equates a shape of a skewed cropped cylinder as shown in figure 5a and 5b. In figure 5a, a measurable 2D-trajectory in the x-z plane through the cropped cylinder with an angle γ is shown. It passes the volume with a distance *q* to the axis of cylinder. The probe volume can be cut into parallelograms in the x'-y-plane, where x' is the coordinate in direction of the trajectory. One of these is shown in figure 5b with a slit width *sl*, the trajectory projection length *b(q)* and the angle ϕ'. ϕ' depends on the off axis angle ϕ and the trajectory angle γ. Here an unavoidable assumption for the 2D measured velocity trajectory is a zero value of the third component in y-direction. Based on this defective assumption, the true burst length bl_{true} in the section *L2-L1* is measured. In the

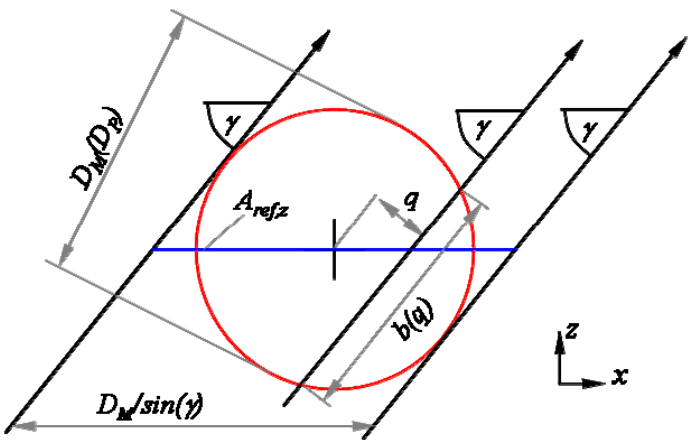

Figure 5a. Trajectories with angle γ through the probe volume with a distance q and on the border to marked the x-dimension of $A_{ref,z}$

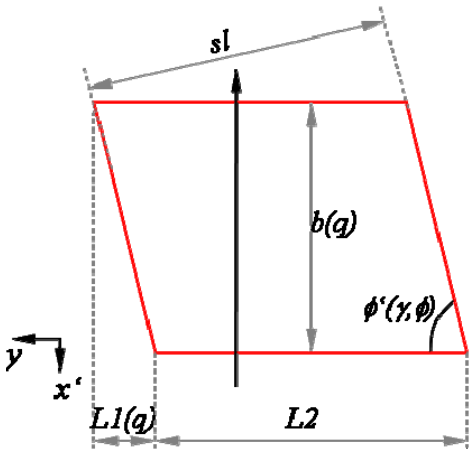

5b. Cross sectional area of the probe volume in the plane of particle trajectory which depends on q and γ

section *L1* on the average only one half of the true burst length will be measured. The smallest measured burst length is defined by the minimum residence time of the particle in the measuring volume. For detection of particles, a minimum residence time is needed by the electronics of the signal processor. The smallest burst length has to be taken into account especially for a small measuring volume and for particles with a high velocity. *L1* and *b* depend on the distance *q* in the probe volume.

With:

$$\phi'_k = \arctan\left(\frac{\tan(\phi)}{\sqrt{1-\sin^2(\gamma_k)}}\right), \tag{2}$$

the minimal burst length:

$$bl_{\min,k} = t_{\min res} \cdot \sqrt{u_k^2 + v_k^2} \tag{3}$$

and

$$b(q) = 2 \cdot \sqrt{\frac{bl_{true}^2}{4} - q^2}\ , \tag{4}$$

the described considerations, referring to a parallelogram as shown in figure 6b combine to:

$$\frac{bl_{mP,k}}{2} = \frac{\frac{b(q)}{2} \cdot \frac{sl}{\sin(\phi'_k)} - \frac{bl_{\min,k}^2}{\tan(\phi'_k)}}{\frac{b(q) - 4 \cdot bl_{\min,k}}{2 \cdot \tan(\phi'_k)} + \frac{sl}{\sin(\phi'_k)}}. \tag{5}$$

Here, k is the kth particle size class of validated particles.

With an integration of $b_{lmP,k}$ over q with the following equation:

$$\int_0^{\sqrt{\frac{bl_{true}^2 - bl_{\min}^2}{4}}} bl_{mP,k}\, dq = bl_{mD,k} \cdot \sqrt{\frac{bl_{true}^2 - bl_{\min}^2}{4}} \tag{6}$$

bl_{true} can be calculated and leads to an expression of the diameter $D_{\text{M,k}}$ of the measuring volume: $D_{M,k} = bl_{true}$. These calculations have to be applied on every size class *k*. Here a further assumption is a statistically uniform distribution of the trajectories trough the probe volume inside a size class. To comply with this, a high number of samples for the size classes are necessary. In this study the size classes with a low number of samples were combined with neighbouring classes if the number of samples is lower then 100.

With the measuring volume diameter D_M the reference area A_{ref} can be calculated. In figure 6a a geometrical consideration for the dependency of D_M and the trajectory angle γ on A_{ref} normal to the *z* –coordinate is shown. The velocity vector spans the area $A_{ref,z}$ around the borderline of the probe volume in the x-y plane. The probe volume is a function of D_M, *sl* and ϕ, and thus A_{ref} can be calculated for each validated particle *i* with:

$$A_{ref,z,i} = \frac{D_{M,k}}{\sin(\gamma_i)} \cdot sl \cdot \sin(\phi). \tag{7}$$

Here the tilting angle as shown in figure 4b has to be taken into account. At this point the flux of validated particles in the direction of the z-coordinate can be calculated.

It has to be mentioned that the drawings in figure 5 are based only on the velocity vectors for the respective particle size. Here the particle size itself is neglected. A consideration of nonzero sizes is much more complex and not included in the flux calculation of this study. If these are taken into consideration, higher values of A_{ref} are expected with increasing particle size. From this follows, that the calculated flux values are little too high.

Results and Discussion

A comparison between the two traverse directions regarding the data and validation rate of test case A is shown in figure 6a and 6b. The data rate of the plot in figure 6a is a little higher than in figure 6b. The best validation rate of both plots is on the outer border outside dense spray region. In this outside area the laser beams aren't disturbed by the annular spray itself. Further downstream the spray density goes down and a better validation rate is realised. But while approaching the flame front at higher z-values, the probability of higher density fluctuations of the gas phase is getting higher and so does the beam steering effect.

With higher y-values the path length of the laser beams in the chamber increases and again so does the beam steering effect. For this reason a better validation rate is observed at lower y-values in figure 6a than in figure 6b. With the better validation rate for the plot in figure 6a, higher values of validated volume flux are expected. This is confirmed as shown in figure 7. Here the locations of the maximum volume flux differ from the locations of maximum data rate of all attempted samples as shown in figure 6. Caused by a very dense spray at the location of highest data rate, fewer particles were registered and also the validation rate goes down. Here the difference between the two plots in figure 7 is small and, hence, it seems that at this location the dense spray effect is dominant. Furthermore it can be concluded, that at this initial location an even smaller measuring volume with higher laser light intensity would be a good solution. The higher validation rate in figure 6a compare to figure 6b suggests that the beam interferences have more effect on the transmittion than on the receiving side.

A comparison of the integrated fuel volume flux with the litered fuel flow for the test case A proved a good consistency. For different z-positions between 10 mm and 25 mm for the traverse ensamble alongside the y-axis, the volume flow comparisons differ between 68 % and 95 %. Smaller values of the integrated volume flow with 40 % were measured in the traverse path at z = 7 mm. Here it was found, that on the position of the maximum data rate at y = -10.5 mm the throughput of the covariance processor is insufficient.

For the test case B with higher pressure and higher air preheat temperature, more severe effects of the dense spray and beam steering were expected. This was confirmed by lower data rates and lower validation rates than test case A. Only 19 % of the litered volume flux was collected on the best downstream position at z = 15 mm. For polydisperse sprays, presentation of velocity data is only useful for defined droplet size intervals. For better comparison to case A, velocity distributions for the drop size interval of 16µm +/- 10%, which is near the Sauter mean diameter of case A, are shown in figure 9b.

Mie- scattering was carried out to support this study with a second measurement method. Using the surface concentration, i.e. culminative droplet surface per unit volume, there is a possibility to compare the PDA data with the Mie data. This is shown in Figure 8a. It is obvious, that the maximum Mie- values are a little bit inwards to the burner axis in comparison with the maximum of surface concentration. Here the PDA method probably

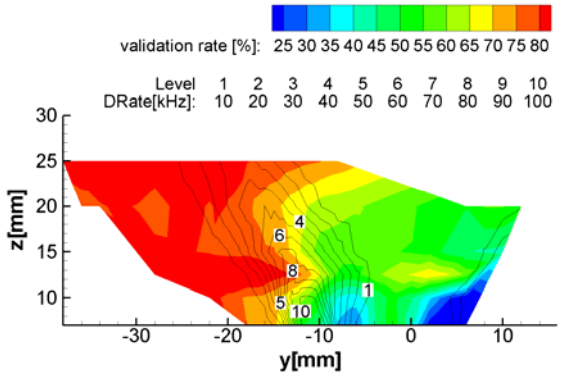

Figure 6a. Test case A: plot of traverse ensemble alongside the y-axis; false colour plots of validation rate of all attempted samples and contour lines of data rate

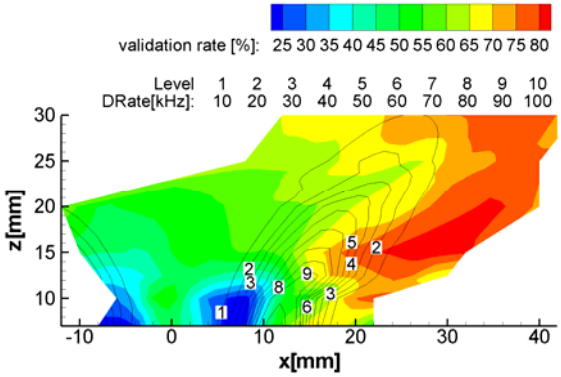

6b. Test case A: plot of traverse ensemble alongside the x-axis; false colour of validation rate of all attempted samples and contour lines of data rate

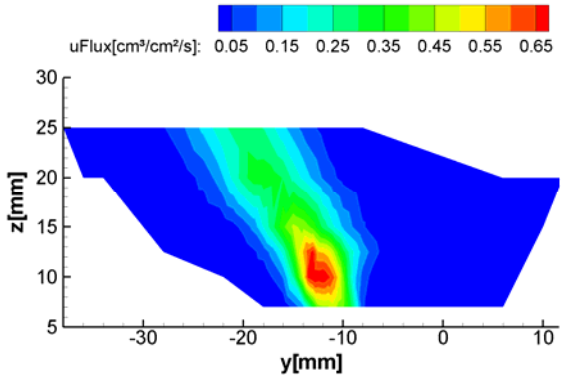

Figure 7a. Test case A: plot of traverse ensemble alongside the y-axis; false colour of volume flux of validated samples in the axial direction

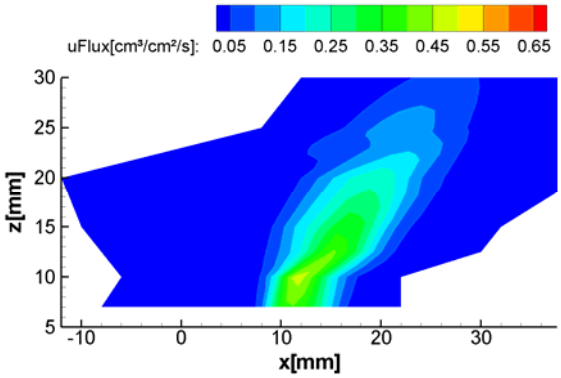

7b. Test case A: plot of traverse ensemble alongside the x-axis; false colour of volume flux of validated samples in the axial direction

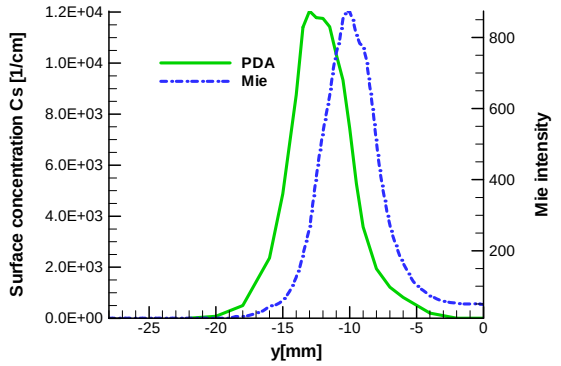

Figure 8a. Test case A: distribution of PDA surface concentration and Mie intensity at axial position z = 10 mm

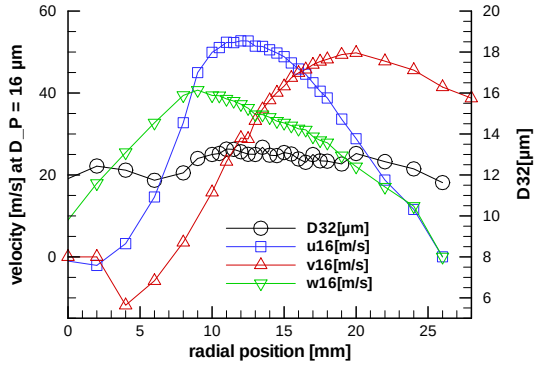

8b. Test case B: distribution of SMD and of velocity for drop sizes of 16 µm +/- 1.6µm at axial position z = 12.5 mm

gives a poorer representation of surface concentration. In particular at positions y > -10 mm the validation rate decreases for the reason of a high number density spray and beam steering as shown in figure 7. In this region the drop size distribution with the smallest values exists as shown in figure 10b and hence a high number of very small drops are not represented in the surface concentration.

An arrival and transit time check of the particles on the positions y > -10 mm shows, that there the dead time of the processor gives rise to beginning loss of data. This leads to the conclusion that at these positions not all drops entering the measuring volume were detected by the PDA.

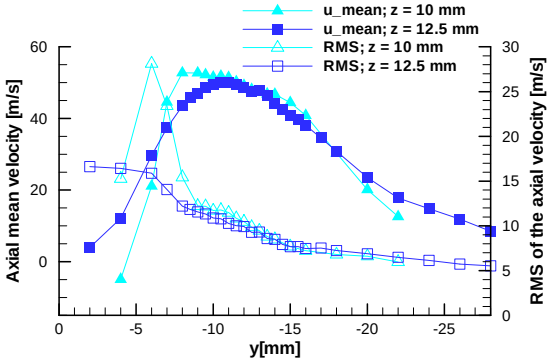

Figure 9a. Test case A: axial mean velocity and RMS profiles of a specific drop size D_P = 16 µm

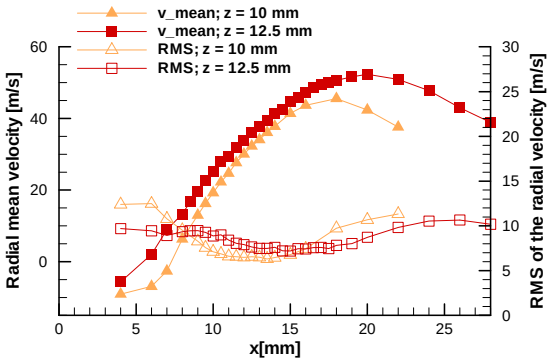

9b. Test case A: radial mean velocity and RMS profiles of a specific drop size D_P = 16 µm

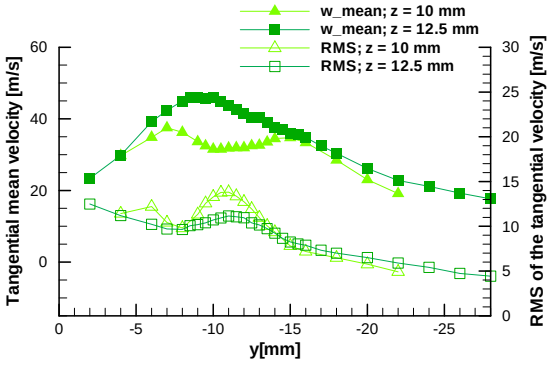

Figure 10a. Test case A: tangential mean velocity and RMS profiles of a specific drop size D_P = 16 µm

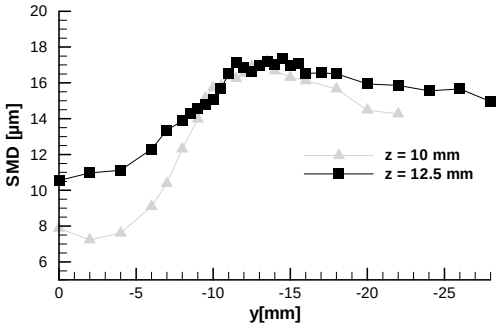

10b. Test case A: SMD profiles

In figure 9 and 10 velocity profiles and SMD distributions represent the initial conditions at axial positions of z = 10 mm and 12.5 mm. In reference to the integrated volume flux with 83 % of the litered fuel volume, the axial position at z = 12.5 mm might be a better position than the z = 10 mm position with 68 % of the litered fuel volume. But at z = 10 mm the maximum u velocity is reached, and therefore the end of the acceleration phase of the droplets. Also the u velocity profile in figure 9a is steeper at the boundary to the recirculation reflecting the exit velocities from the burner with higher fidelity. A notable effect is displayed by the dropsize profiles of 10b at z = 10 mm and even more so on figure 8b: Compared with earlier results on atmospheric sprays, as reported for instance in [1], the variation of mean size along the radius is small. Tangential separation is delayed by the lower density ratio of fuel to air, and hence also dispersion at least during the acceleration phase of the droplets up to z = 10 mm.

Conclusions

A measurement setup strategy to measure the initial conditions of spray for the difficult case of high droplet number density in a combustor with a lifted flame and at elevated pressure was demonstrated. The resulting findings are summarized as follows:

- The choice of transmitting optics to get a small measuring volume has the advantage of higher laser intensity and a decrease of dense spray effects.
- With a conventional receiving optic it is possible to choose a large off axis angle to minimize the fluctuating refractive index at higher temperature without a 2π- ambiguity as it would be for the planar part for a dual receiving optic. A 2D-volume flux calculation algorithm adapted to the geometrical situation with the consideration of the off axis angle dependency on the probe volume led to a good consistence of the calculated volume fluxes compared to the litered fuel fluxes.

With a comparison of the data rate and validation rate alongside the different beam path directions in the chamber it is possible to compare the influence of beam steering and dense spray effect with respect to their influence on the transmitting and receiving side. For this study a higher dependency of the transmitter beam path was identified.

The smallest drops of all were measured inside the annular spray cone. Here long beam path lengths in the chamber through the dense spray led to a lower signal to noise ratio and a high number of small droplets were not detected by PDA. At regions like this the Mie-scattering is a useful addition to PDA for an extensive spray analysis.

At higher pressure and higher air preheat temperatures the disturbances are higher. It was found, that for a case with an air pressure of 1 MPa and a preheat temperature of 650 K the calculated volume flux data was much lower than for the 0,4 MPa case and hence the fuel flux measurement is no longer quantitative. Nevertheless the accuracy of the measurement of velocity and drop size is still reasonable.

Acknowledgements

This work received funding from the European Community through the project TIMECOP-AE (Project # AST5-CT-2006-030828). It reflects only the author's views and the Community is not liable for any use that may be made of the information contained therein.

Nomenclature

A	area [m^2]
AFR	air to fuel ratio by mass [-]
b	2D-projected trajectory length trough the probe volume [µm]
bl	burst length [µm]
Cs	surface concentration [1/cm]
D	diameter [µm]
$Flux$	volume flux [$cm^3 \cdot cm^{-2} \cdot s^{-1}$]
ϕ	off axis angle [°]
λ	wave length [nm]
m	relative refractive index between air and fuel [-]
m_{mol}	molar mass of air [$g \cdot mol^{-1}$]
$\dot{m}$	mass flow [$kg \cdot s^{-1}$]
p	air pressure [Pa]
q	radial distance in a size class probe volume [µm]
R	specific gas constant of the air [$J \cdot kg^{-1} \cdot K^{-1}$]
sl	slit width of the receiving optic [µm]
T	temperature [K]
te	elapsed time of a measure point [s]
u	axial velocity [$m \cdot s^{-1}$]
v	radial velocity or second measured velocity component [$m \cdot s^{-1}$]
w	tangential velocity [$m \cdot s^{-1}$]
ρ	density [$kg \cdot m^{-3}$]
σ	surface tension [$kg \cdot s^{-2}$]

Subscripts

air	gas phase air
i	validated sample
k	refers to size class
liq	liquid fuel kerosene Jet A-1
M	measuring volume
$meas$	measured value
mD	mean value refers to q
mP	mean value refers to parallelogram
P	particle
ref	reference
$true$	rectified value
w	wall

References

[1] Behrendt, T., and Hassa, C., *AGARD Conference proceedings 598*, paper Nr. 5 1997.
[2] Behrendt, T., Carl, M., Heinze, J., and Hassa C., *Atomization and Sprays 16*, 475-491 (2006).
[3] Ikeda, Y., Hirohata, T., and Nakajima, T., *8th International Symposium on Applications of Laser Technology to Fluid Mechanics*, Lissbon, Portugal, Paper No. 2.6, 1996.
[4] Tsushima, S., Akamatsu, F., Katsuki, M., Mizutani, Y., and Cho, Y.D., *8th International Symposium on Applications of Laser Technology to Fluid Mechanics*, Lissbon, Portugal, Paper No. 2.4, 1996.
[5] Rachner, M., "Die Stoffeigenschaften von Kerosin Jet A-1", Mitt. 98-01, DLR, Cologne, Germany, 1998, ISSN 1434-8462.
[6] BSA Flow Software Vers. 4.10 Installation and User's Guide, Dantec Dynamics A/S, Publication no.: 9040U5733, 2006
[7] Saffmann, M., *Aplied optics 26*, No. 13, 2592-2597 (1987).
[8] Brandt, M., Rachner, M., and Schmitz , G., *Combustion Science and Technology*, No. 98-04-27, (1998).